Applied Surface Science Advances 13 (2023) 100365

Contents lists available at ScienceDirect

Applied Surface Science Advances

journal homepage: www.sciencedirect.com/journal/applied-surface-science-advances

Electrochemical corrosion behavior of tantalum coated 316L stainless steel by D.C. Magnetron sputtering for orthopedic applications

Dileep Pathote *, Dheeraj Jaiswal, Vikrant Singh, C.K. Behera

Metallurgical Engineering Department, Indian Institute of Technology (BHU) Varanasi-221005, India

ARTICLE INFO

Keywords:
316L stainless steel
Tantalum coating
Corrosion
Orthopedic applications

ABSTRACT

The austenitic stainless steel type 316L was engineered with a thin multilayer of tantalum with a thickness of 1.504μm, 3.893 μm and 6.083μm and a duration of 15, 30 and 60 minutes, respectively, by the DC Magnetron Sputtering. Electrochemical behaviors of all three samples were investigated by potentiodynamic and electrochemical impedance spectroscopy techniques. Simulated body fluid was used as the corrosive medium for the electrochemical measurement. The highest corrosion resistance was obtained for the sample subjected to 60 minutes of Ta deposited on 316L S.S. according to EIS measurements, and the lowest corrosion rate of 0.0047 mm/year was obtained for the same sample according to the PD measurements. All the measurements were carried out after the determination of open circuit potential (OCP) at 37℃ with 1 ±°C. All the samples were then characterized by scanning electron microscopy (SEM) to observe the morphology of coating after corrosion. The number of corrosion pits observed from the SEM micrograph was much less on the three coated samples compared to the bare sample. X-ray Photoelectron Spectroscopy (XPS) was used to identify the chemical states of coated and bare 316L SS. Ta4f is present as oxidation states in Ta coated stainless steel 316L, whereas Ta4f is the main species examined along with other elements (C1s, N1s, O1s, Cr2p, Fe2p, Ni2p, and Mo3d). It was also observed that there was strong adhesion between substrate and Ta-coating. After the potentiodynamic studies, results show a significant improvement in corrosion resistance attributed to the strong, stable oxide layer formation.

1. Introduction

Surgical metal implants are a structural component used very specifically for the strengthening of a bone. A group of implants consists of bolt and nut compression plates attached to the bone. This is particularly useful when traditional methods (excluding implants) could cause the atrophy of cartilages and joining of the body to be exclusively long [1]. Austenitic stainless steel is widely used in the field of osteosynthesis because of its outstanding mechanical properties: resistance to corrosion and value for money. However, the formation of chlorides (Cl^-) at high levels along with the regular human body temperature could create localized corrosions such as pitting, cramping and fatigue of the cargo by using this type of stainless steel. Due to machining imperfections and crevices, formation takes place, which results in fatigue cracks formation [2]. Surgical implants are typically made of metals such as cobalt-chromium alloys, austenitic stainless steel and titanium and its alloys. Austenitic stainless steels are the most used metallic materials because of their comparative ease of manufacturing, low cost, and good corrosion resistance. Austenitic stainless steels, on the other hand, are prone to localized corrosion [3]. Metal ions with 316L stainless steel have been suggested to be toxic to estrogenic cells and affect their spread and differentiation. In specific concentrations, the usual behavior of osteoblast-like cells can be disturbed by products of stainless steel corrosion; dental and surgical alloy biocompatibility is primarily associated with corrosion. The corrosion resistance of biocompatible alloys is significant for human body implants not merely because it determines a device's life but because corrosion products in the living organism are harmful. The cell metabolism of corrosion products was detected. This means that corrosion current may be impaired by cell behavior [4]. The body is not considered hospitable to an implanted metal alloy with a high pH of saline electrolyte of approximately 7.4 and a temperature of 98.6°F (37°C). While chloride solutions are well known to be among the most aggressive and corrosive to metals, the ionic composition and protein concentration of body fluids make the new understanding of biomedical corrosion even more difficult. Alloy composition variations can lead to subtle differences in mechanical, physical or electrochemical

* Corresponding author.
E-mail address: dileeppathote.rs.met20@itbhu.ac.in (D. Pathote).

https://doi.org/10.1016/j.apsadv.2022.100365
Received 19 May 2022; Received in revised form 27 October 2022; Accepted 25 December 2022
Available online 28 December 2022

Table 1
Orthopaedic characteristics of stainless steel metallic implant [1] and [13].

Design-nation	Principal Alloying Element (wt.%)	Primary Utilizations	Advantages	Disadvantages
F-138 ASTM	Ni(12-14), Mo(2-4), Cr(17-20), and Fe (Bal.)	Temporary devices (hip nail, screw, fracture plates) used for T.H.R.s stem in the U.K. (Rich N2), joint arthroplasty, osteosynthesis.	Availability processing, cost, fatigue resistance, corrosion resistance, high wear resistance	High modulus with long term behavior, high friction coefficient, ascetic loosing, generation of wear debris

Table 2
The chemical composition of 316L stainless steel in wt.%.

Material	Cr	Ni	Mo	Mn	C	S	P	Si	Fe
316L SS	17.5	13.6	2.27	1.39	0.13	0.005	0.003	0.015	Balanced

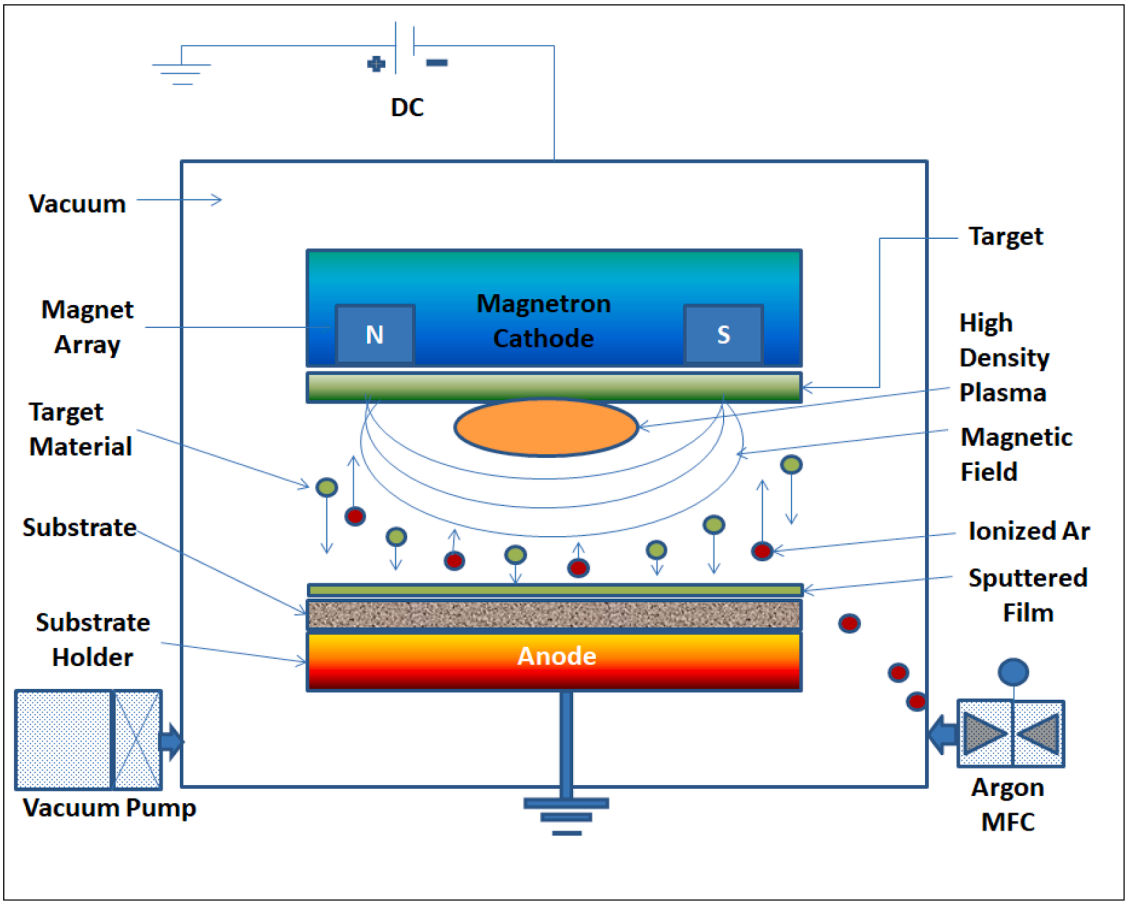

Fig. 1. Systematic direct current magnetron sputtering (DCMS) process.

Table 3
Composition of simulated body fluid at 7.4pH [14].

Constituents	NaCl (gram)	$NaHCO_3$ (gram)	KCl (gram)	$(CH_2OH)_3.CNH_3$ (gram)	$MgCl_2.6H_2O$ (gram)	1.0 HCl (ml)	$CaCl_2$ (gram)	Na_2SO_4 (gram)
Amount in 1000 ml	8.035	0.355	0.225	6.118	0.10	39	0.292	0.072

characteristics [5]. Four main groups were divided into orthopedic implants: osteosynthesis (stabilization and bone fixation); joint substitutions; Unconventional modular tumor implants; spine implants [6]. While human body pH levels are generally maintained at 7.0 levels, the pH value changes from 3 to 9 for many reasons, including accidents, biological imbalances, chronic illness, infection, etc., and pH levels near implants typically vary from 5.3 to 5.6 post-surgery [7–12]. Temporary implants such as flats and screws and permanent implants used to substitute the hip, knee, spin, shoulder, toe, finger etc., are included in the implants. Cutting corrosion in shielded areas at the screw/plate interface and in the underheads of the fastening tors and pitting corrosion of the S.S. implants is the mechanism for corrosion in temporary implants. The leading cause is wear, which, in turn, accelerates corrosion. The deposition of resistant corrosion coating on their surfaces is one of the most popular and economical ways to improve corrosion resistance in metallic structures. Direct current magnetron sputtering

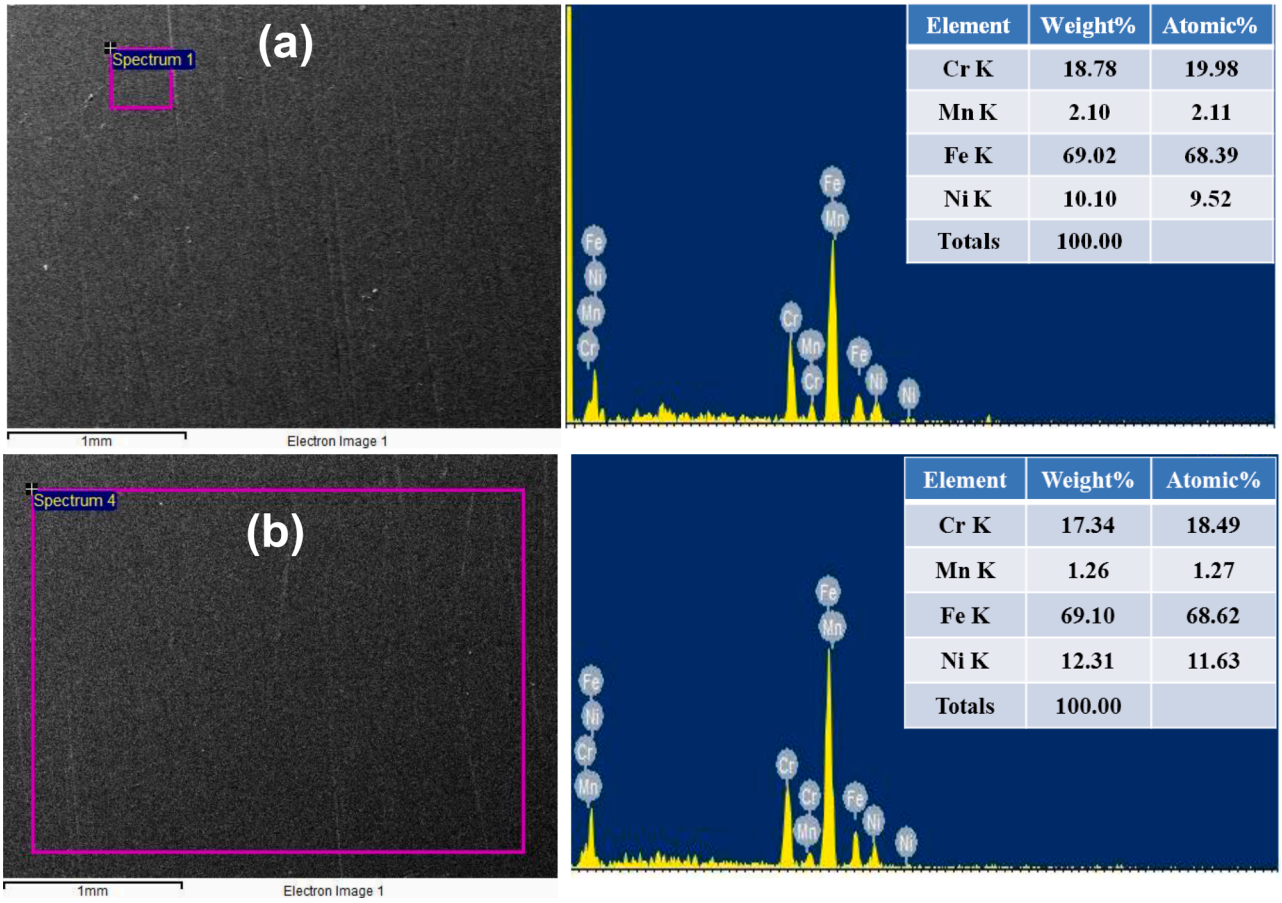

Fig. 2. EDX images of bare samples (a) EDX image of bare 316L S.S. at spectrum-1 (b) EDX image of bare 316L SS at spectrum-4.

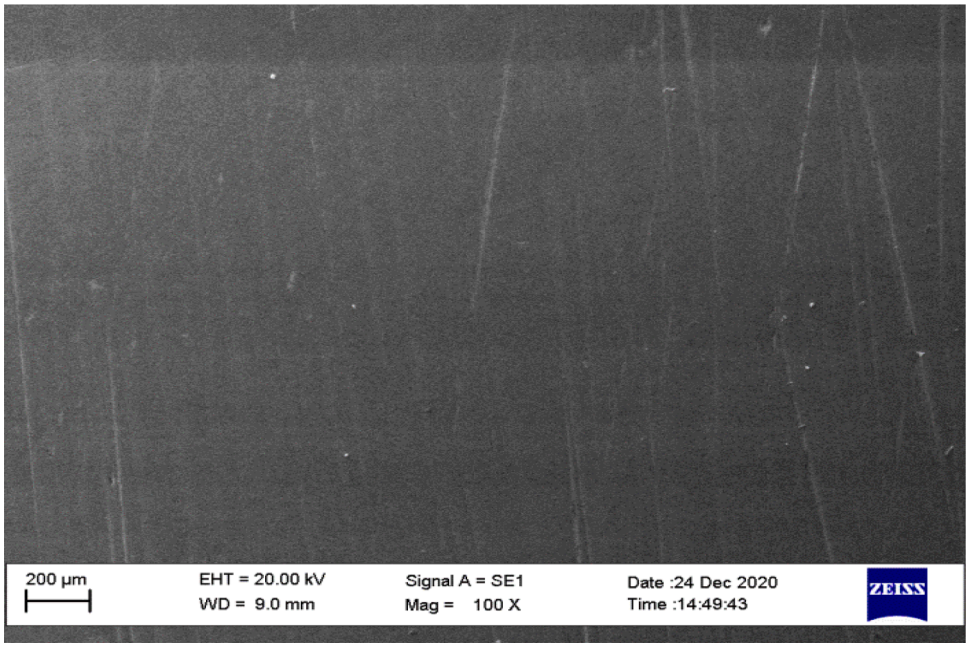

Fig. 3. SEM image of bare 316L SS.

deposition is one of the physical vapor deposition (PVD) techniques that have been quickly developed for industrial applications over the past few decades, including the production of tough, wear, low friction, corrosion-resistant and decorative filings and other thin shaped systems with specific electrical and optical characteristics. Sputtering is a cost-effective method, and a highly purified and homogeneous finish can be deposited in large areas with strong substrate adhesion. Characteristics of stainless steel metallic implants are summarized in the Table 1.

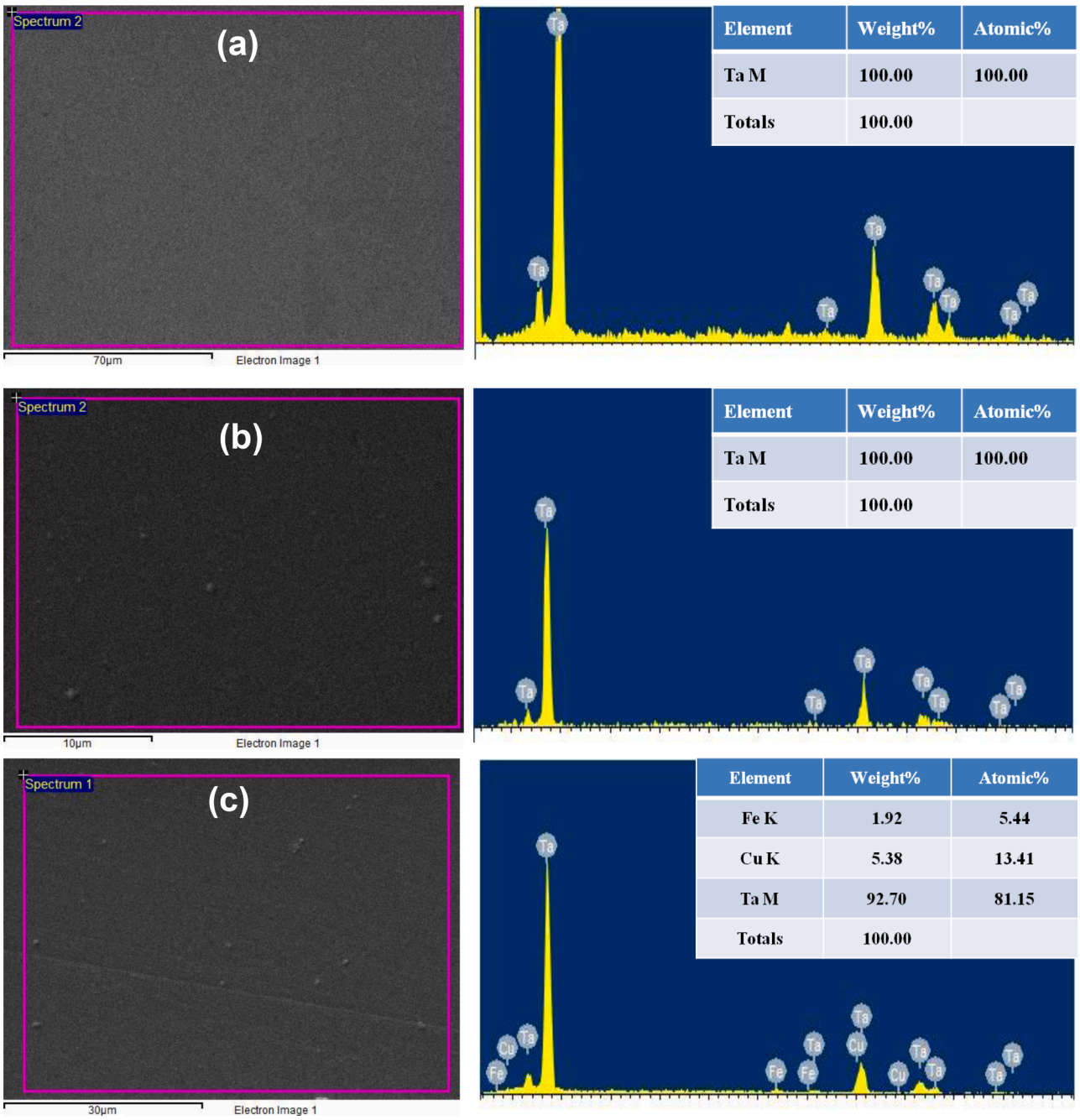

Fig. 4. EDX images of Ta-coated 316L S.S. samples (a) 15 min. Ta-coating (b) 30 min. Ta-coating (c) 60 min. Ta- coating.

In this study, stainless steel type 316L is coated with tantalum (Ta) with a thickness of 1.504µm, 3.893 µm, and 6.083µm duration of 15, 30, and 60 minutes, respectively, by using DC magnetron sputtering system. Then metallurgical characterization was done by Optical Microscopy (OM), Scanning Electron Microscopy, Energy Dispersive X-ray Spectroscopy, and X-ray photoelectron spectroscopy (XPS) for both Ta-coated and bare 316L SS after investigating electrochemical corrosion behavior. In order to use the long-term applications without internal implant failure and effective performance (especially Ta-coated 316L SS) to the orthopedic applications.

2. Experimental procedure

2.1. Materials and sample preparation

Austenitic stainless steel 316 L was received from Mishra Dhatu Nigam Limited (MIDHANI), Hyderabad, India. The Stainless steel type 316L had dimension of 472 × 775 × 20mm. The typical chemical compositions as received are given in Table 2.

The required number of samples (four in this case) of dimensions 20 × 20 × 2 mm were prepared from the received sample of 316L SS with the help of a table moving CNC wire-cut EDM machine. Samples were mirror-polished before deposition of Ta coating using emery paper up to 1600 grit, followed by washing with distilled water and hot air blow-drying. The specimens were then ultrasonically cleaned with acetone for 10 minutes to achieve good adhesion with the coating. Optical

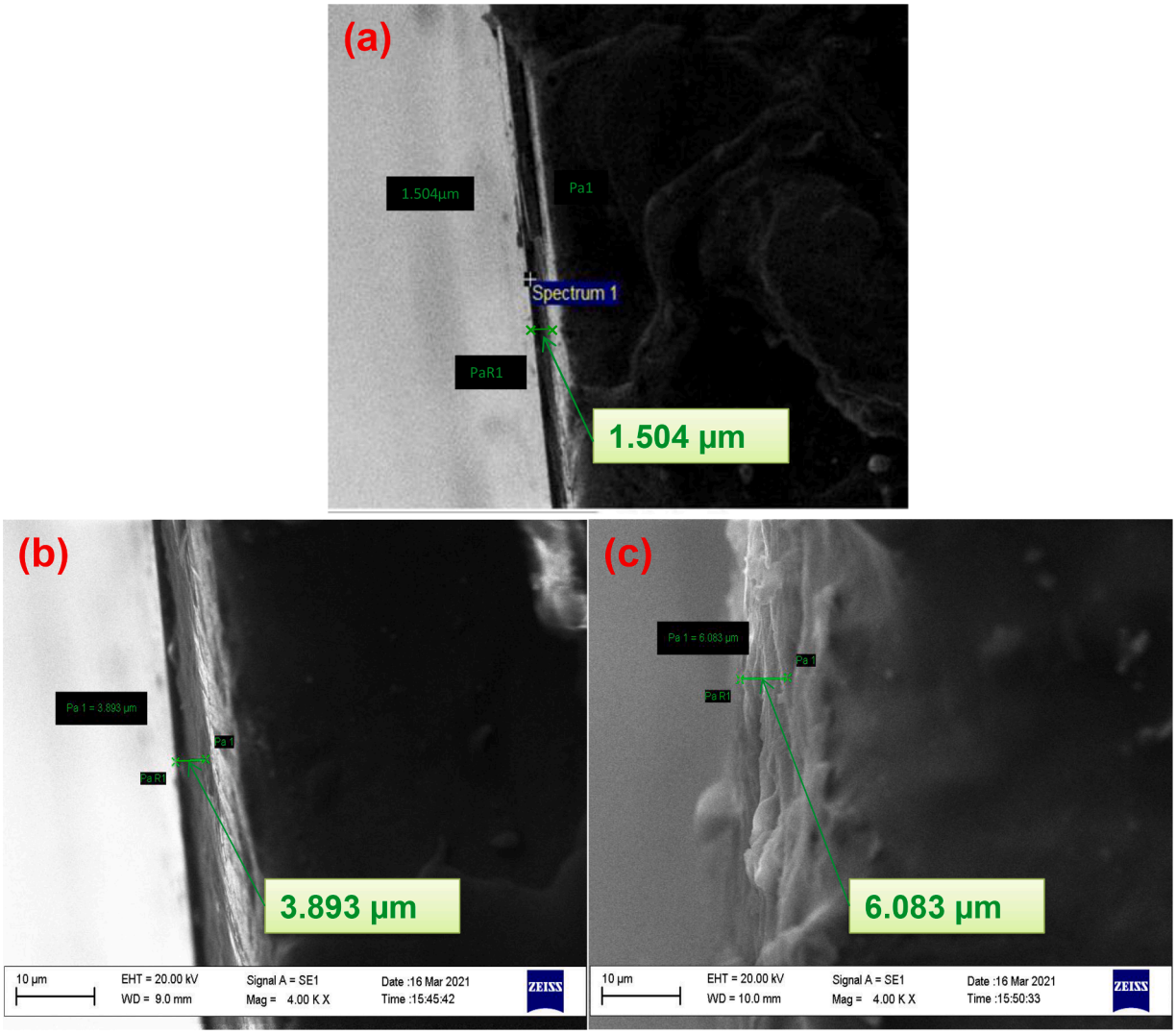

Fig. 5. SEM images before corrosion of Ta-coated 316L SS (a) 15 min. Ta-coating (b) 30 min. Ta-coating (c) 60 min. Ta- coating.

Table 4
Ta-coated thickness by DC magnetron sputtering on 316L with time interval.

Sample	Coating Time (minutes)	Thickness of coating (µm)
316L SS	15	1.504±0.042
316L SS	30	3.699±0.194
316L SS	60	6.083±0.028

microscopy was used to check the substrate constantly to ensure the microstructure of the sample surface.

2.2. Deposition of tantalum

Direct current magnetron sputtering (DCMS) is a thin film physical vapor deposition (PVD), The coating process in which the target material to be coated is bombarded with ionized gas molecules, causes atoms to be "sputtered" off into the plasma. These vaporized atoms are subsequently deposited as a thin-film on the substrate to be coated when they condense.

Fig. 1 shows the systematic DCMS process. Thin-film was deposited with high purity sputter tantalum target (99.95% Ta) with a dimension of 55.8mm diameter and 3.175 mm thickness onto stainless steel 316L (20×20 mm^2) by the DCMS. Constant argon (Ar) gas flows with a current rate of 0.15 amp were used as the optimal deposition condition. The chiller temperature was maintained at 20℃ and a voltage range of 270-276V. Magnetron source shutters were provided for pre-ionizing. Special magnetics fulfil the requirement of uniformly sputtering. To accommodate a single target, argon gas flow was uniformly distributed inside the chamber for the thin film preparation of tantalum. Tantalum was deposited on 316L SS specimens (3 nos.) for 15minutes, 30 minutes and 60 minutes, by DCMS to achieve a certain level of variation in thickness. For all the proceedings, the subtract holder's distance to the target was kept at 70mm, its rotation speed at 7-9 rpm and its working temperature at 180℃. The base pressure and working pressure of the chamber were maintained below 5×10^{-4} Pa and 5×10^{-1} Pa, respectively. The proportion of argon gas with a flow rate of 16 sccm and deposition pressure was controlled by a mass flow controller (MFC).

2.3. Microstructure analysis

Before the Ta coating was observed all three specimens 316L S.S. surface used an optical microscope (OM, LeicaZ6 APO) and were investigated by the energy dispersive X-ray spectrometry (51N1000 – EDS System, Oxford Instruments Nanoanalysis) and Scanning Electron Microscopy (SEM, ZEISS MA 15/18, UK) and after the coating also it was characterised. The sample was then coated with tantalum for 15, 30, and 60 minutes by the D.C. sputtering machine; the 316L S.S. was examined to observe surface morphology by scanning electron microscopy (SEM)

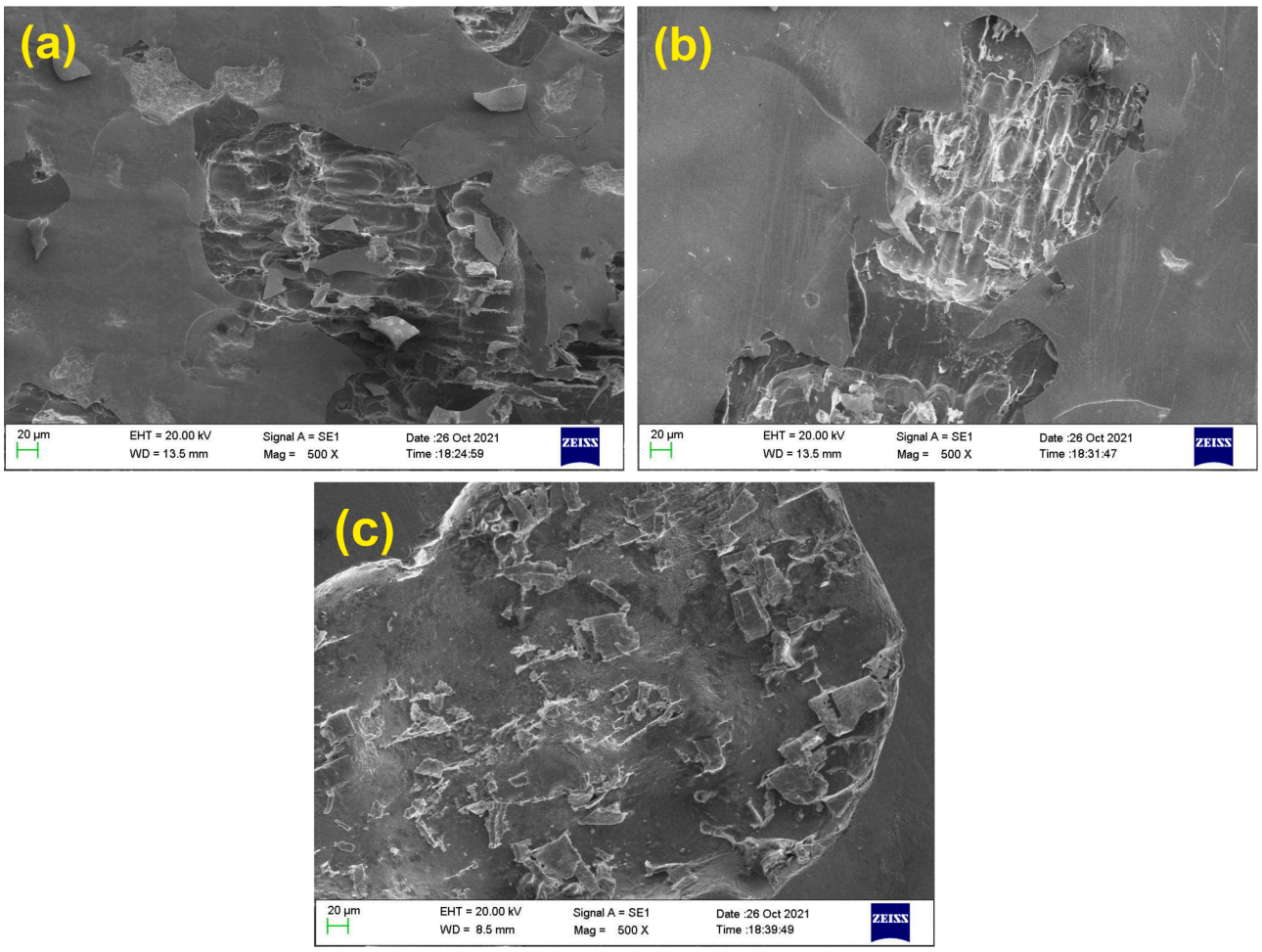

Fig. 6. SEM images after corrosion of Ta-coated 316L SS (a) 15 min.Ta-coating (b) 30 min. Ta-coating (c) 60 min. Ta-coating.

and, the chemical composition of the samples was determined by the energy dispersive X-ray spectrometry (EDS). X-ray Photoelectron Spectroscopy (K-alpha, Thermo Fisher Scientific) was used to identify the chemical states and elemental composition of the Ta coated and bare 316L SS. The surface nano analysis XPS system used a 150W non-monochromatic Al Kα radiation of 1486.6 eV. The XPS survey and core spectra of Ta, Fe, O, Cr, Mo, Ni, Mn, and C were determined.

2.4. Electrochemical corrosion analysis

Electrochemical measurement was characterized by potentiodynamic polarization and, an electrochemical impedance spectroscopy (EIS) test. The samples were tested in simulated body fluid (SBF) were prepared by using the high purity chemicals given in Table 3. The typical three-electrode system, in which 316L S.S. act as a working electrode, platinum electrode (Pt) acts as an auxiliary electrode and silver chloride electrode (Ag/Ag.Cl) acts as a reference electrode was used for the electrochemical corrosion measurement.

3. Results and discussion

3.1. Characterization of Bare 316L SS

The energy dispersive X-ray analysis of the bare 316 L samples indicates a high content of Cr, Ni, Mn, Fe etc., as the components of 316L SS shown in Fig. 2 of the EDX images. From the SEM micrographs of the 316L S.S. bare sample in Fig. 3 it was observed that no surface irregularities are present at 100X magnification. It is essential to make sure that no defects are present on the surface before tantalum coating and corrosion studies.

3.2. Characterization of Ta-Coated 316L SS

The energy dispersive X-ray analyses of the Ta coated 316 L samples were carried out for all three samples. It was observed that only Ta was present, which confirms the uniform coating of Ta on the surface of 316L SS as shown in Fig. 4. Further Ta-coated 316L S.S. samples were examined using S.E.M. to determine surface morphology which is essential to assess before corrosion studies. Fig. 5 is the SEM images of Ta-coated 316L S.S. from 15 min. to 60 min before corrosion. The results presented in Fig. 5b (3.893 µm) suggest that the average thickness of coating is 3.699±0.194 µm.The same micrographs were used to determine the thickness of the Ta coating. The absences of any significant pits was confirmed by SEM The thicknesses of the coating for three samples are listed in Table 4. The thickness was uniform and increased with the increase of time of deposition of the coating. The minimum thickness was 1.504 µm for 15 minutes of deposition, and the maximum was 6.083 µm for 60 minutes of deposition. All the SEM micrographs are presented in Fig. 5 for 200X and 400X magnifications.

As-sputtered multilayer Ta/Ta_2O_5 thin film had a shiny appearance, as illustrated in Fig. 6 and appeared in exquisite black due to the effect of argon flow rate ratio and deposition power on surface morphology and cross-sectional microstructure. After the potentiodynamic polarization test, however, this original appearance faded to a bland white. Features of the as-sputtered and annealed Ta/Ta_2O_5, such as shape and compositions, were compared using SEM microstructural and elemental

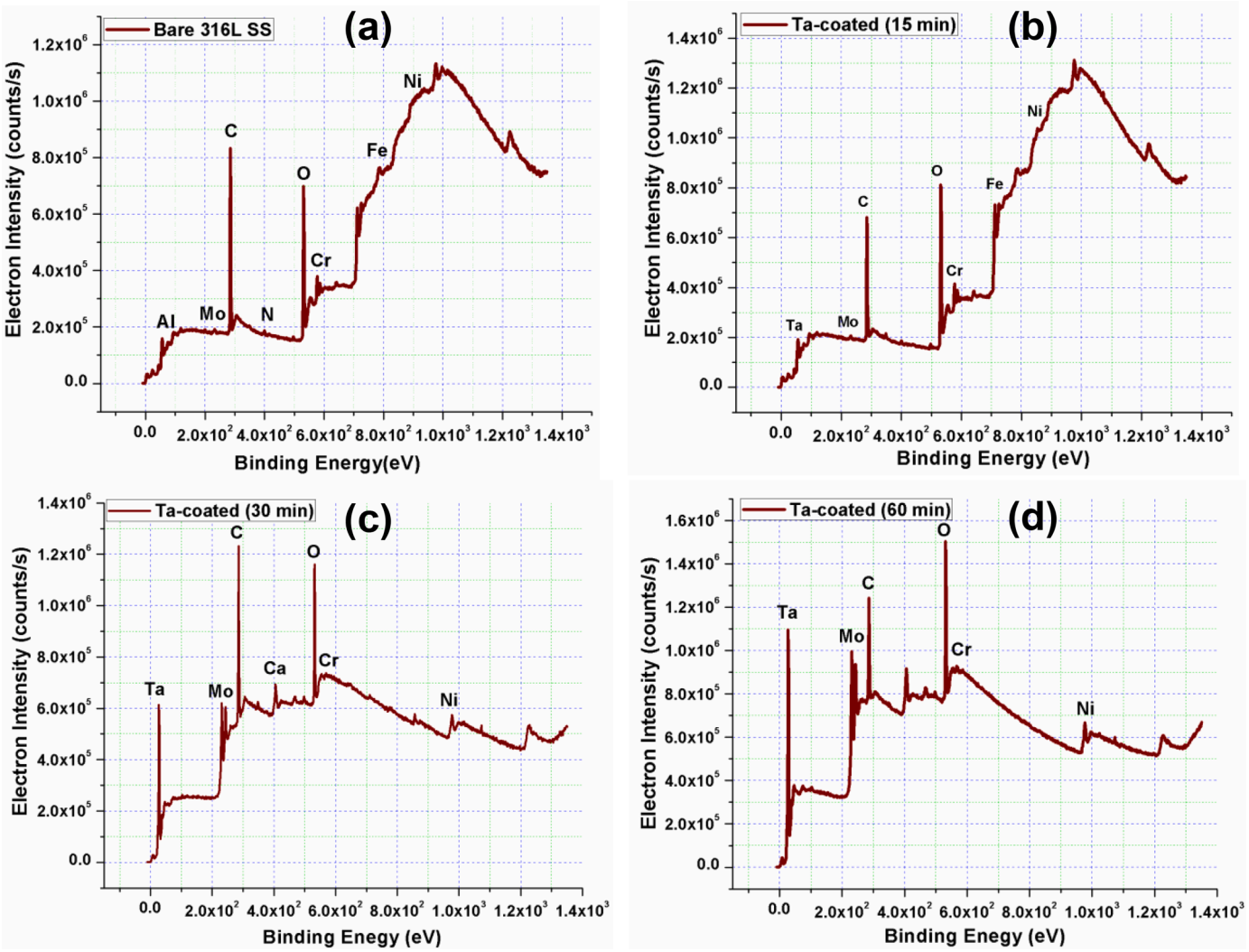

Fig. 7. XPS spectra of 316L Stainless steel (a) Bare (b) 15min. Ta-coated (c) 30min.Ta-coated (d) 60min.Ta-coated.

analyses. Fig. 6 shows the surface morphology of as-sputtered thin film samples with their cross-sectional microstructure under various magnetron sputtering experimental settings. Tantalum serves as an effective seed layer for Ta film over the 316L S.S., resulting in the production of a fine-grained structure with a smoother surface. Furthermore, the tantalum system has a consistent surface shape, as seen in Fig. 6, While multiple cracks and discontinuities can be seen in the single-layer Ta film. This is typically what causes the metastable Ta to form at the interface. Tantalum is available in two distinct phases: an α -phase, which is a stable body centred cubic structure (bcc) and a β-phase with a tetragonal metastable structure that can be transformed into a β-phase by thermal treatment at high temperatures (750-950°C) [15,16–18].

3.3. X-ray Photoelectron Spectroscopy (XPS)

In Fig. 7 (a–d), the XPS broad scan survey spectra and core spectra for each element contained in the coating are plotted, and images are presented. In Fig. 7, the presence of characteristic peaks in relative binding energies of elements (Ta4f, C1s, N1s, O1s, Cr2p, Fe2p, Ni2p, and Mo3d) suggests that tantalum was successfully incorporated into the coating matrix. Before the corrosion test, the Ta4f core level of spectra located at binding energies from 2466.3 eV, 2337339.21 eV, and 4213045.02 eV, simultaneously 0.01%, 6.99%, and 12.27% atomic percentages achieved Ta coated stainless steel type 316L (15 min., 30 min., and 60 min.) respectively.

It is important to note that a pure Ta film's Ta4f spectrum has a significant shoulder at energy doublet, implying that the deposited film seems to be primarily metallic Ta. For bare 316L stainless steel, XPS spectra show the peaks of Ni, Fe, Cr, O, C, N, Mo, Al, and Ta coated for 15 min. sample represents the peaks of the Ni, Fe, Cr, O, C, Mo, and Ta, Ta coated for 30 min. sample shows the peaks of the Ni, Cr, O, Ca, C, Mo, and Ta, Ta coated for 60 min. sample shows the peaks of the Ni, Cr, O, C, Mo, and Ta.

XPS spectra of 316L Stainless steel show which main peaks O, C, Fe, Ni, and Mo are present. In Fig. 8, the XPS results of Chromium (Cr 2p), Aluminium (Al 2p), Molybdenum (Mo 3d), Nickel (Ni 2p), oxygen (O1s), carbon (C1s), Iron (Fe 2p), and Nitrogen (N 1s) spectra of bare stainless steel type 316L are presented. According to the findings, the examined surface layer contains both chromium metal and compounds. Clear peaks of Molybdenum, nickel, carbon, and iron can also be seen. Apart from oxides and hydroxides, the final one, with a lot of oxygen in the passive layer, can generate iron, chromium sulfide, and phosphates. Cr 2p and Fe2p fits were performed to better understand the chemical composition of the surface layer, as shown in Fig. 8. According to our findings, the change in chemical composition on the uppermost surface is closely related to corrosion resistance. After coating, the quantity of Cr in unoxidized stainless steel susceptible to corrosion is drastically reduced. It's essential to compare the Fe and O composition changes linked to product corrosion after coating. Table 5 shows the compounds

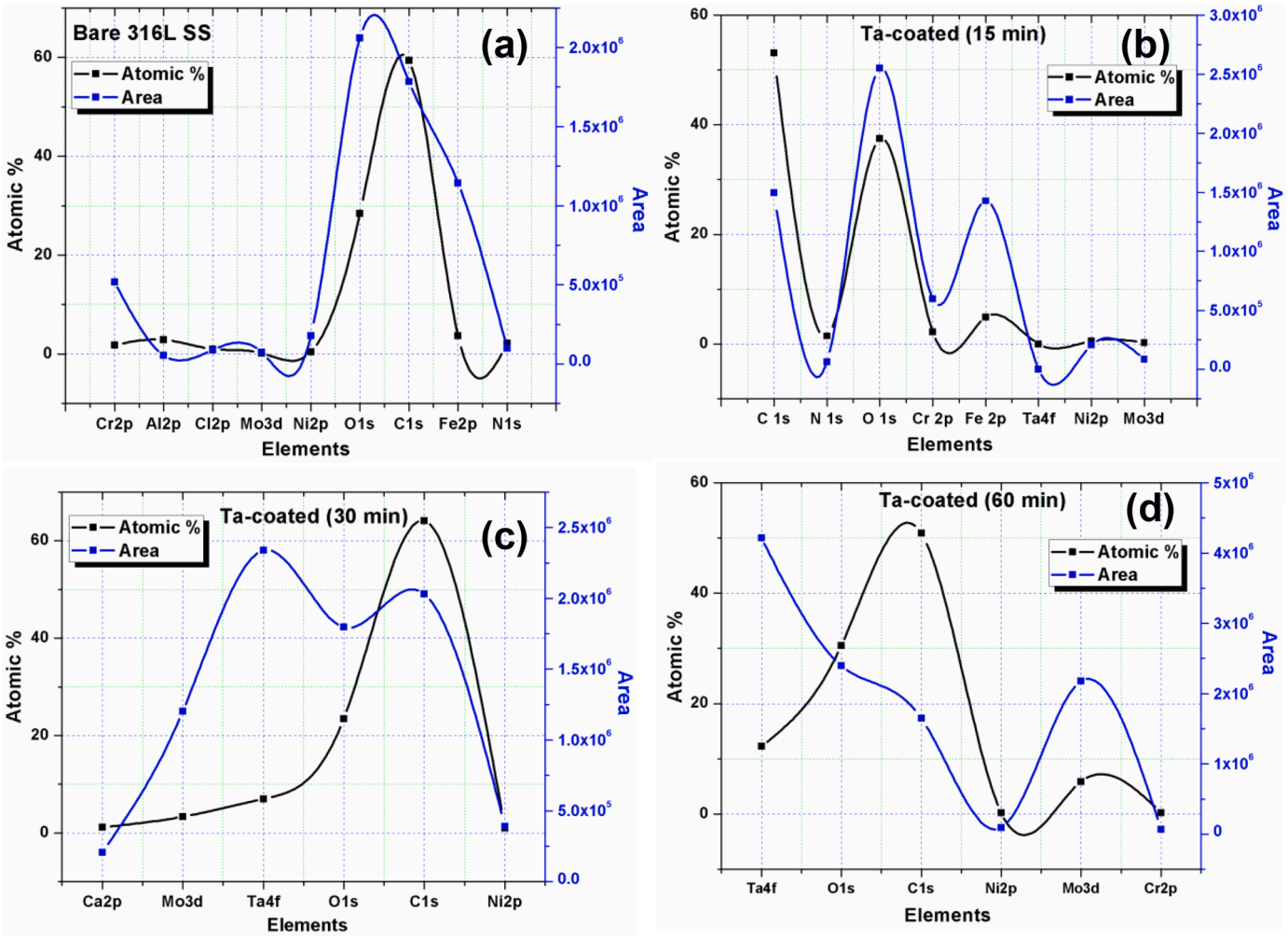

Fig. 8. XPS spectra (elemental and atomic %) of 316L Stainless steel (a) Bare (b) 15min. Ta-coated (c) 30min.Ta-coated (d) 60min.Ta-coated.

Table 5
Compounds and Binding Energy (BE) of bare and coated 316L stainless steel.

Bare 316l SS		Ta coated (15 min)		Ta coated (30 min)		Ta coated (60 min)	
Compounds	BE (eV)	Compounds	BE (eV)	Compounds	BE (eV)	Compounds	BE(eV)
Cr2p	594.08	C 1s	298	Ca2p	360.08	Ta4f	32.08
Al2p	76.58	N 1s	410	Mo3d	238	O1s	537.58
Cl2p	210.08	O 1s	540.45	Ta4f	32.58	C1s	298.08
Mo3d	238	Cr 2p	594	O1s	541.08	Ni2p	882
Ni2p	882	Fe 2p	735.54	C1s	298.08	Mo3d	238
O1s	538.08	Ta4f	28	Ni2p	882.08	Cr2p	592
C1s	294.58	Ni2p	882	-	-	-	-
Fe2p	737.08	Mo3d	238	-	-	-	-
N1s	410.08	-	-	-	-	-	-

and binding energy (BE) of bare and coated 316L stainless steel. These findings suggest that the initial amount of Cr, largely present in Cr_2O_3 before coating, has a significant impact on corrosion resistance.

3.4. Electrochemical corrosion analysis

3.3.1. Open circuit potential study

An open circuit potential (OCP) measurement was performed for 1 hour to ensure that the specimen's working surface was stable, and monitoring of 316L SS bare and Ta-coated 316L S.S. in simulated body fluid at pH of 7.4 and temperature of 37°C was completed. Potential was established between the working electrode and the environment in relation to a reference electrode.

3.3.2. Electrochemical impedance spectroscopy study

An EIS test was performed by frequency sweeping the range from the initial 1000 Hz to the final 10 Hz at 0.2V potential against OCP at a scan rate of 10mV/Minute for 60 minutes logarithmic and 100 points in S.B. F. at 37°C for all the samples (316L S.S. bare, and Ta-coated 316L S.S. from 15 to 60 Minutes), respectively. To obtain the corrosion rate and corrosion resistance data, the EIS tests were analyzed with CView (CS studio, version 5.2) and ZView (CS studio, version 5.2) software. Fig. 9 shows the experimental data of the equivalent electric circuit of bare and tantalum coating samples. The proposed model contains three-time constraints;, the solution resistance (R.S.);, constant phase element-1 (CPE-1) connected in series; constant phase element-2 (CPE-2) connected in parallel alongwith resistance (R) of the electrolyte and

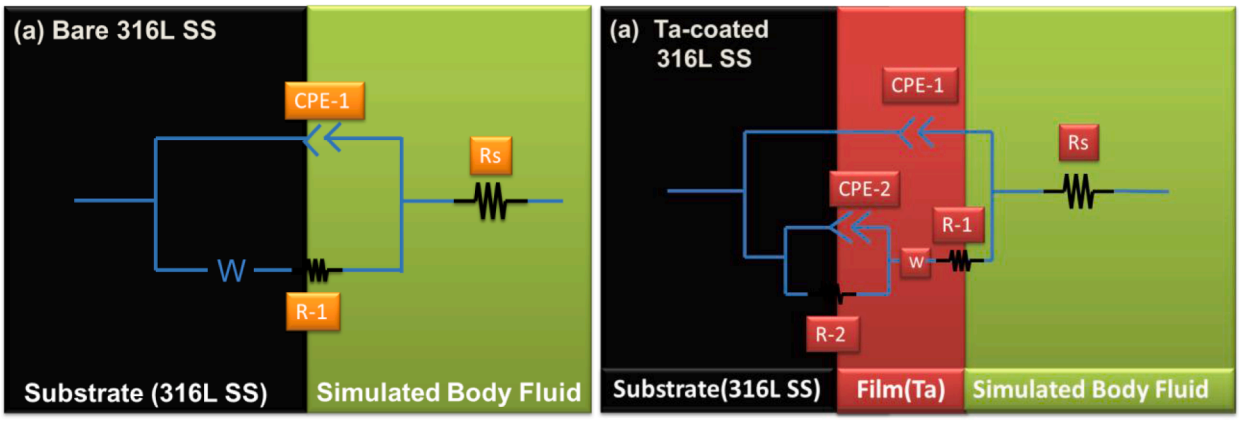

*R_s = Solution Resistance, CPE = Constant Phase Element, R_1= Resistance of Porous product layer of corrosion, R_2= Resistance of alloy interface & product of corrosion, and W = Warburg Impedance

Fig. 9. Equivalent electric circuit (EEC) for a) 316L SS (bare) and b) Ta-coated-316L SS.

Table 6
Parameters of the equivalent electrical circuit model bare and coated samples in 7.4 pH.

Samples	R_s Ωcm^2	R_1 Ωcm^2	CPE_1 Y_1*10^{-6} Ωcm^{-2}s^n	n_1	R_2 Ωcm^2	CPE_2 Y_2*10^{-9} Ωcm^{-2}s^n	n_2	R_w Ωcm^2	χ^2 * 10^{-4}
316L BARE	73.22	1878	0.85	0.75	-	-	-	6123	0.2496
Ta-Coating (15Min.)	89.76	3864	0.40	0.81	10170	1.57	0.76	25.94	0.2412
Ta-Coating (30Min.)	90.40	40931	3.82	0.85	20.58	1.94	0.86	18965	0.2641
Ta-Coating (60Min.)	80.80	61291	1.63	0.77	46418	0.72	0.79	23990	0.2818

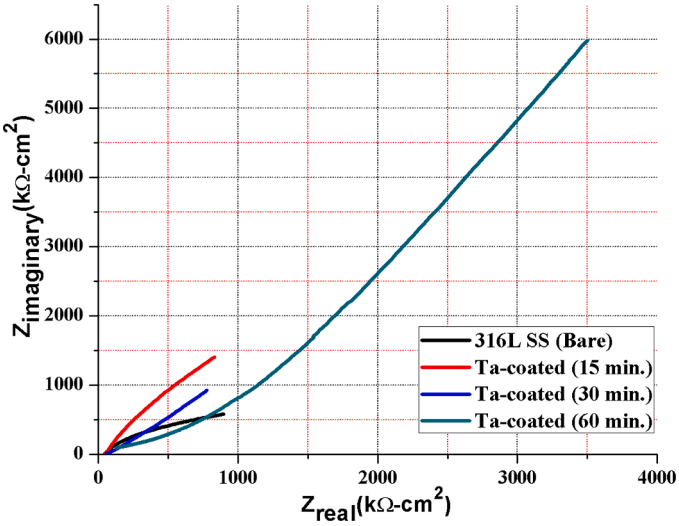

Fig. 10. Nyquist plot for bare and Ta-coated 316L SS in SBF at 7.4 pH.

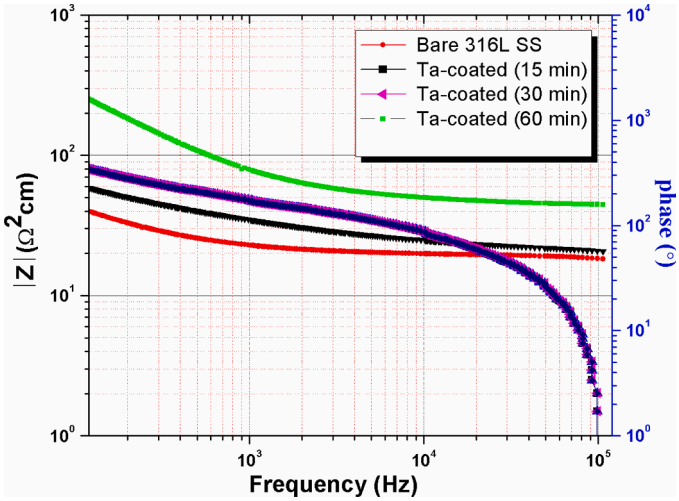

Fig. 11. Bode plot for bare and Ta-coated 316L SS in SBF at 7.4 pH.

Warburg impedance (W). Furthermore, at the base of micro pores, the capacity of both bare and coated samples arranged in parallel could be assumed to be equal so that only a single element is used [19]. The constant phase element (C.P.E.) can be used to simulate the non-ideal behavior of a capacitor [20–27]. It could be defined by two values, CPE-T (T) and C.P.E. (P). The C.P.E. is defined as:

$$Z = 1 / \left[T_{(jw)}{}^{n}\right]$$

Where $j=\sqrt{-1}$, $w= 2\pi f$ is an angular frequency (rad/s) and f is the frequency (Hz), n is known as a dimensionless number related to non-uniform current distribution because of the surface inhomogeneity and roughness which varies between 0.75 and 1.

The anodic oxidation of tantalum coating in anodic solution leads to the formation of Ta_2O_5 [28,29]. The corresponding cathodic half-reaction is [30–39]:

$$Ta_2O_5 + 10H^+ + 10e^- \leftrightarrow 2Ta + 5H_2O \qquad [E = 0.75 vs. SHE]$$

Fig. 9 for the equivalent electric circuit demonstrates the bare and coated samples, in which R_s represents the solution resistance, CPE_1 and R_1 represent capacitance and resistance of porous product layer of corrosion, and CPE_2 and R_2 belong to the capacitance and resistance of electrical double layer between alloys interface and product of the corrosion. Table 6 shows the parameters of the equivalent electrical circuit (EEC) model bare and coated samples in 7.4 pH. The EEC is used to explain whether a process operates when there are two-time constants: a high-frequency (H.F.) time constant (CPE_1-R_1) and a low-frequency (L.F.) time constant (CPE_2-R_2).

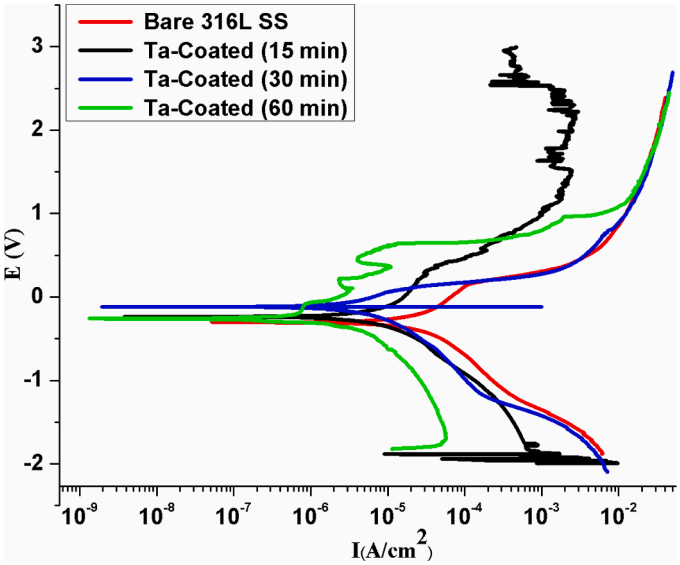

Fig. 12. Potentiodynamic polarization curve for bare and Ta-coated 316L SS.

Table 7
Polarization parameter for bare and Ta-coated 316L S.S. in 7.4pH at 37°C.

Sample	βa (mv)	βc (mv)	I_0 (A/Cm^2)	Eo (V)	CR (mm/y)
316L SS (Bare)	586.52	484.99	5.519E-06	-0.2375	0.2053
Ta-coated (15 min.)	270.69	255.13	25.043E-06	-0.1171	0.0603
Ta-coated (30 min.)	1710.70	195.67	8.1438E-07	-0.2585	0.0196
Ta-coated (60 min.)	145.18	4164.90	1.9635E-07	-0.0034	0.0047

Fig. 10 depicts the Nyquist plot for bare and Ta-coated 316L S.S. in SBF at 7.4 pH. The EEC parameter values were calculated using the experimental data. The HF time constant's physical meaning is to speed up charging/discharging and charge transfer operations, which are represented by a parallel combination of the double layer/space charge capacitance (CPE_1) and the charge transfer resistance (R_1). The LF time constant (CPE_2-R_2), on the other hand, is associated with slower mass transport phenomena in the oxide phase, such as electroactive ions migration through the use of the generated passivity. Fig. 11 shows the Bode plot for bare and Ta-coated 316L SS in SBF at 7.4 pH.

3.3.3. *Potentiodynamic study*

Tafel extrapolation of the relevant polarization parameters revealed polarization curves for the bare and Ta coated 316L stainless steels shown in Fig. 12. It has been observed that I_{corr} decreases with an increase in thickness of coating, which indicates that the corrosion product also acts as protection from further corrosion. The E_{corr} for 316L S.S. was greater in the coated sample than that of the bare sample. This indicates that the spontaneity of corrosion is less for the coated sample than that of bare samples. It was observed that 316LSS has minimum breakdown potential among all other samples. Corrosion parameters and performance of all the samples are given in Table 7 at a pH of 7.4 and at 37°C. The potentiodynamic polarization curve was obtained according to D.O.E. specifications for anodic corrosion [40–47] shown in Fig. 12. As a result, it has been established that the corrosion protection provided by this Ta-based coating increases with time from 15 minutes up to 60 minutes. It should also be noted that the Bode diagram's high frequency region contains data about coating flaws and changes in surface area. To verify the stability of passivation film at a given voltage range of about 3V, because the change in corrosion potential is dependent on a change in one or both of the anodic and cathodic reactions, the long-term change in corrosion potential (open-circuit potential) represents a change in a corrosion system. An increase in corrosion potential, for example, might be attributable to a decrease in the anodic reaction due to the formation of a passive layer. A sharp increase in current density is located when a potential is reached at 2.7693E-1, signalling the passivation film breakdown after the constant potential from 6.8407E-2 to 9.2607E-4. An empirical equation to evaluate the porosity (P) of the coatings and protective efficiency is [48,49];

$$\mathbf{P} = \frac{\mathbf{RpS\ (Subtract)}}{\mathbf{Rp\ (Coating/\ Subtract)}} \times \left(\nabla E_{\frac{corr}{p}}\right) \quad (1)$$

Here P is the total coating porosity, R_ps is the polarization resistance of the substrate material, Rp is the calculated polarization resistance of the coated system, ΔE_{corr} is the potential difference between the bare substrate steel and the corrosion potential of the coated steel and β is the anodic Tafel slope of the substrate [49].

Calculated polarization resistance (Rp) of the coated system is:

$$\mathbf{Rp} = \frac{\beta\mathbf{a} * \beta\mathbf{c}}{\{2.3\mathbf{x\ icorr\ x}\ (\beta\mathbf{a} + \beta\mathbf{c})\}} \quad (2)$$

Here βa is the anodic Tafel constant, and βc is the cathodic Tafel constant. Protective efficiency (Pi) of the coating is determined from the polarization curve by the following equation;

$$\mathbf{Pi} = 100 * \frac{1 - \mathbf{iCorr}}{\mathbf{i0Corr}} \quad (3)$$

Here i_{corr} and i°_{corr} are the corrosion current densities in the presence and absence of the coating, respectively.

Fig. 12 shows Tafel curves generated using the Tafel polarization method after a 1 h holding period of coated and untreated AISI 316 L austenitic stainless steel in SBF medium. Because the Icorr values of the AISI 316 L austenitic steel were greater than the uncoated state and the Rp values were substantially lower than the uncoated condition, the corrosion resistance of the Ta coated samples in the SBF medium appears to be lower than expected.

4. Conclusion

Ta coating on 316L SS was performed by DC magnetron sputtering techniques for time durations of 15, 30 and 60 minutes. It was observed that the thickness of the Ta coating increased with time confirmed by SEM. The thickness of the samples was 1.504μm, 3.699 μm and 6.083μm for 15, 30 and 60 minutes of deposition, respectively. Electrochemical corrosion measurements were carried out for all the coated and bare samples in simulated body fluid at 37°C. From the electrochemical impedance spectroscopy (EIS) measurement, it was observed that the corrosion resistance of the coated sample is basically due to the resistance of the corrosion product and the coating/metal interface. The highest resistance is exhibited by the sample coated for 60 minutes and the lowest for the bare sample. From the potentiodynamic measurements, it was observed that the corrosion rate decreases with an increase of Ta thickness. The highest corrosion rate of 0.2053 mm/y was obtained for 316L SS (bare), and the lowest value of 0.0047 mm/y for the sample with 60 minutes of Ta coating. The surface characterizations after corrosion for the entire sample were completed by SEM and EDX. SEM and EDX revealed that there was a stable coating between coating and substrate. Some tantalum oxide was present on the corroded surface without the presence of any other substances. This confirms the exhibition of good corrosion resistance of Ta coating on 316L SS. The corrosion performance of the Ta coated samples in simulated body fluid is much better than the stainless steel 316L. XPS measurements were used in the experiment to clarify further the chemical state and composition of the prepared Ta coatings and determine the source of the coating's strong resistance to corrosion against bare 316L SS. Together in a wide range of processing parameters, meaningful XPS results of

austenitic AISI 316L stainless steel tantalum coating have been acquired. The Fe 2p region significantly differs in XPS results depending on surface treatment (bare and coated). For good peak fitting of the 2p XPS spectra of iron and chromium, the 2p doublet peaks should be fitted together; the energy loss tail of each component should be taken into account. The survey spectra can provide helpful information by considering peak background and differences between 2p and 3p peaks. Tantalum films on metal surfaces enhance corrosion potentials and lower current densities, mainly passive current density, then 316L stainless steel. Consequently, the corrosion rate of Ta coated 316L stainless steel is lower than that of bare 316L stainless steel.

Conflict of Interest

"The authors declared that have no conflict of interest".

Data Availability

Data will be made available on request.

Acknowledgements

The authors gratefully acknowledge the funding from the Science and Engineering Research Board (SERB) of India (Project No. R&D/SERB/MET/19-20/04), and for the research experimental facilities of the ''Indian Institute of Technology Banaras Hindu University'' (IIT-BHU), Varanasi-221005 India.

Supplementary materials

Supplementary material associated with this article can be found, in the online version, at doi:10.1016/j.apsadv.2022.100365.

References

[1] MM Dewidar, HC Yoon, JK. Lim, Mechanical properties of metals for biomedical applications using powder metallurgy process: a review, Met. Mater. Int. 12 (3) (2006) 193–206.
[2] Y Sawa, T Horiuchi, A Kishida, T Masuzawa, M Nishimura, E Tatsumi, Y. Tomizawa, H Watanabe, The year in review, J. Artif. Organs 10 (2) (2007) 53–59.
[3] MH Fathi, Mortazavi V. Tantalum, Niobium and titanium coatings for biocompatibility improvement of dental implants, Dentel Res. J. 4 (2) (2007) 74–82.
[4] R Singh, NB. Dahotre, Corrosion degradation and prevention by surface modification of biometallic materials, J. Mater. Sci. Mater. Med. 18 (5) (2007) 725–751.
[5] DC. Hansen, Metal corrosion in the human body: the ultimate bio-corrosion scenario, Electrochem. Soc. Interface 17 (2) (2008) 31–34.
[6] GE. Novikova, Introduction to corrosion of bioimplants, Prot. Met. Phys. Chem. Surf. 47 (3) (2011) 372–380.
[7] B Aksakal, ÖS Yildirim, H. Gul, Metallurgical failure analysis of various implant materials used in orthopedic applications, J. Fail. Anal. Prev. 4 (3) (2004) 17–23.
[8] D. Pathote, D. Jaiswal, V. Singh, C.K. Behera, Optimization of electrochemical corrosion behavior of 316L stainless steel as an effective biomaterial for orthopedic applications, Mater. Today Proc., no. xxxx (2022) 1–5, https://doi.org/10.1016/j.matpr.2022.02.501.
[9] V. Singh, D. Jaiswal, D. Pathote, C.K. Behera, Drop calorimetric measurement of In-Zn system for lead-free solder applications, Mater. Today Proc. 57 (2022) 285–288, https://doi.org/10.1016/J.MATPR.2022.02.601.
[10] M.R. Kumar, V. Singh, V.K. Rai, D. Jaiswal, C.K. Behera, Investigation on mixingheat effect of bi-in and in-sn system at 730 K, Mater. Today Proc. 18 (2019) 2917–2923. https://doi.org/10.1016/j.matpr.2019.07.161.
[11] V.K. Rai, M.R. Kumar, V. Singh, D. Jaiswal, C.K. Behera, Analysis of corrosionbehavior and its characterization of in-sn-bi alloy, Mater. Today Proc. 18 (2019) 2322–2328. https://doi.org/10.1016/j.matpr.2019.07.015.
[12] D. Jaiswal, D. Pathote, V. Singh, C.K. Behera, Electrochemical behaviour of lead-free Sn-In-Al solders alloys in 3.5 wt% NaCl solution, Mater. Today Proc. (2022), https://doi.org/10.1016/j.matpr.2022.02.315.
[13] ZA Uwais, MA Hussein, MA Samad, N Al-Aqeeli, Surface modification of metallic biomaterials for better tribological properties: a review, Arab. J. Sci. Eng. 42 (11) (2017) 4493–4512.
[14] N. Eliaz, Corrosion of metallic biomaterials: a review, Materials 12 (3) (2019).
[15] YJ Lee, TH Lee, DY Kim, HH Nersisyan, MH Han, KS Kang, Y.J.Lee Shin, J. H, Microstructural and corrosion characteristics of tantalum coatings prepared by molten salt electrodeposition, Surf. Coat. Technol. 235 (2013) 819–826, https://doi.org/10.1016/j.surfcoat.2013.09.007 [Internet]Available from:.
[16] ZL Yuan, DH Zhang, CY Li, K Prasad, CM Tan, LJ Tang, A new method for deposition of cubic Ta diffusion barrier for Cu metallization, Thin. Solid. Films 434 (1–2) (2003) 126–129.
[17] D. Jaiswal, D. Pathote, V. Singh, C.K. Behera, Effect of Al addition onelectrochemical behavior of Sn-0.7Cu-xAl lead-free solders alloys in 3.5 wt% NaClsolution, J. Mater. Eng. Perform. (2022). https://doi.org/10.1007/s11665-022-06771-y.
[18] D. Pathote, D. Jaiswal, V. Singh, R.K. Gautam, C.K. Behera, Wear behavior and microhardness studies of tantalum (ta)-coated 316L stainless steel by DC magnetron sputtering for the Orthopedic Applications, J. Mater. Sci. 57 (45) (2022) 21039–21056. https://doi.org/10.1007/s10853-022-07939-6.
[19] M Alishahi, F Mahboubi, Mousavi Khoie SM, M Aparicio, E Lopez-Elvira, J Méndez, R. Gago, Kopasz, P John, Benjamin, G Thomas, Deanna Wang Schenk, Lixia Li, Lei Shen, Jing Gao, Haili Sun, Juncai Wang, Heng Cao, Yang Lee, Y.J. Lee, T. H. Kim, D.Y. Nersisyan, H.H. Han, M.H. Kang, K.S. Bae, K.K. Shin, Y.J. Lee, J. H. Yuan, Z.L. Zhang, D.H. Li, C.Y. Prasad, K. Tan, C.M. Tang, L.J. Contreras, A. León, C. Jimenez, O. Sosa, E. Pérez, R. Cavigliasso, G.E. Esplandiu, M. J. Macagno, V.A. Resetic, A. Jaric, B. Michaelis, Alexander, High conductivity and anti-corrosive tantalum surface modified ferritic stainless steel bipolar plate for direct ethanol fuel cell, J. Appl. Electrochem. 14 (11) (2019) 768–774, https://doi.org/10.1016/j.surfcoat.2013.09.007 [Internet]Available from:.
[20] R Alias, R Mahmoodian, K Genasan, KM Vellasamy, M Hamdi Abd Shukor, T Kamarul, Mechanical, antibacterial, and biocompatibility mechanism of P.V.D. grown silver–tantalum-oxide-based nanostructured thin film on stainless steel 316L for surgical applications, Mater. Sci. Eng. C 107 (March 2019) (2020), 110304, https://doi.org/10.1016/j.msec.2019.110304 [Internet]Available from:.
[21] Y Zhang, Y Zheng, Y Li, L Wang, Y Bai, Q Zhao, Xiaoling Cheng Xiong, Yan Tang, Zhihui Deng, Yi Wei, Shicheng, Tantalum nitride-decorated titanium with enhanced resistance to microbiologically induced corrosion and mechanical property for dental application, PLoS One 10 (6) (2015) 1–22.
[22] D Cristea, I Ghiuță, D. Munteanu, Tantalum based materials for implants and prostheses applications, Bull. Transilv. Univ. Braşov. 8 (57) (2015) 151–158.
[23] GS Kaliaraj, V Vishwakarma, A Ramadoss, D Ramachandran, AM. Rabel, Corrosion, haemocompatibility and bacterial adhesion behavior of TiZrN-coated 316L S.S. for bioimplants, Bull. Mater. Sci. 38 (4) (2015) 951–955.
[24] DB Kumar, R Nagalakshmi, KG Muthurajan, V Rajasekar, S. Parthasarathi, Corrosion behaviour of S.S. 316L in different medium, J. Chem. Pharm. Sci. (9) (2015) 284–286, 2015-April.
[25] Hou L Da, Li Z, Y Pan, MI Sabir, YF Zheng, L Li, A review on biodegradable materials for cardiovascular stent application, Front. Mater. Sci. 10 (3) (2016) 238–259.
[26] P Mahmoudi Hashemi, E Borhani, MS Nourbakhsh, A review on nanostructured stainless steel implants for biomedical application, Nanomed. J. 3 (4) (2016) 202–216 [Internet]Available from: http://nmj.mums.ac.ir/article_7574.html%0Ahttp://nmj.mums.ac.ir/article_7574_5c59f5d2fd08d4b425c231704a4a388e.pdf.
[27] L Kunčická, R Kocich, TC. Lowe, Advances in metals and alloys for joint replacement, Prog. Mater Sci. 88 (2017) 232–280.
[28] L Wang, L Li, J Shen, H Gao, J Sun, H Wang, Yang Cao, High conductivity and anti-corrosive tantalum surface modified ferritic stainless steel bipolar plate for direct ethanol fuel cell, Results Phys. 14 (March) (2019), 102394, https://doi.org/10.1016/j.rinp.2019.102394 [Internet]Available from:.
[29] GE Cavigliasso, MJ Esplandiu, VA. Macagno, Influence of the forming electrolyte on the electrical properties of tantalum and niobium oxide films: An E.I.S. comparative study, J. Appl. Electrochem. 28 (11) (1998) 1213–1219.
[30] Michaelis A. Valve Metal, Si and ceramic oxides as dielectric films for passive and active electronic devices. Vol. 10, Electrochemical Surface Modification Thin Films, Functionalization and Characterization, 2008, pp. 1–106.
[31] N Hassan, NA Abdel Ghany, Corrosion of biomaterials: anodic treatment and evaluation of 316L stainless steel in simulated body fluid, Corros. Eng. Sci. Technol. 52 (4) (2017) 267–275, https://doi.org/10.1080/1478422X.2016.1267932 [Internet]Available from:.
[32] P Guzmán, W Aperador, L. Yate, Enhancement of the pitting corrosion resistance of AISI 316LVM Steel with Ta-Hf-C/Au bilayers for biomedical applications, J. Nanomater. 2017 (2017).
[33] A Bekmurzayeva, WJ Duncanson, HS Azevedo, D. Kanayeva, Surface modification of stainless steel for biomedical applications: Revisiting a century-old material, Mater. Sci. Eng. C 93 (2018) 1073–1089, https://doi.org/10.1016/j.msec.2018.08.049 [Internet]Available from:.
[34] Santos GA dos, The importance of metallic materials as biomaterials, Adv. Tissue Eng. Regen. Med. Open Access 3 (1) (2017) 300–302.
[35] DD Kumar, GS. Kaliaraj, Multifunctional zirconium nitride/copper multilayer coatings on medical grade 316L S.S. and titanium substrates for biomedical applications, J. Mech. Behav. Biomed. Mater. 77 (2018) 106–115, https://doi.org/10.1016/j.jmbbm.2017.09.007 [Internet]Available from:.
[36] H Ghorbani, A Abdollah-Zadeh, A Poladi, M. Hajian, Pulsed DC- plasma assisted chemical vapor deposition of α-rich nanostructured tantalum film: Synthesis and characterization, Int. J. Eng. Trans. A 30 (4) (2017) 551–557.
[37] CW Kang, FZ. Fang, State of the art of bioimplants manufacturing: Part I, Adv. Manuf. 6 (1) (2018) 20–40, https://doi.org/10.1007/s40436-017-0207-4 [Internet]Available from:.

[38] AC Hee, Y Zhao, S.S. Jamali, A Bendavid, PJ Martin, H. Guo, Characterization of tantalum and tantalum nitride films on Ti6Al4V substrate prepared by filtered cathodic vacuum arc deposition for biomedical applications, Surf Coat. Technol. 365 (2017) (2019) 24–32, https://doi.org/10.1016/j.surfcoat.2018.05.007 [Internet]Available from:.

[39] D Jaiswal, V Singh, D Pathote, CK. Behera, Electrochemical behaviour of lead-free Sn–0.7Cu–xIn solders alloys in 3.5 wt% NaCl solution, J. Mater. Sci. Mater. Electron 32 (18) (2021) 23371–23384, https://doi.org/10.1007/s10854-021-06824-3 [Internet]Available from:.

[40] JP Kopasz, TG Benjamin, D. Schenk, 2017 Bipolar Plate Workshop Summary Report, 2017, pp. 1–37.

[41] AP Manso, FF Marzo, X Garicano, C Alegre, A Lozano, F. Barreras, Corrosion behavior of tantalum coatings on AISI 316L stainless steel substrate for bipolar plates of P.E.M. fuel cells, Int. J. Hydrog. Energy 45 (40) (2020) 20679–20691.

[42] L Geyao, D Yang, C Wanglin, W. Chengyong, Development and application of physical vapor deposited coatings for medical devices: a review, Procedia CIRP 89 (2020) 250–262, https://doi.org/10.1016/j.procir.2020.05.149 [Internet] Available from:.

[43] H Ghorbani, A Abdollah-zadeh, F Bagheri, A. Poladi, Improving the bio-corrosion behavior of AISI316L stainless steel through deposition of Ta-based thin films using PACVD, Appl. Surf. Sci. 456 (May) (2018) 398–402, https://doi.org/10.1016/j.apsusc.2018.06.154 [Internet]Available from:.

[44] M Talha, CK Behera, S Kumar, O Pal, G Singh, OP. Sinha, Long term and electrochemical corrosion investigation of cold worked AISI 316L and 316LVM stainless steels in simulated body fluid, R.S.C. Adv. 4 (26) (2014) 13340–13349.

[45] C.E. J, J.M. T, J.C. J, H.I.M. Walenkamp G, J. P, Modern orthopaedic implant coatings — their Pro's, Con's and evaluation methods, Mod. Surf. Eng. Treat. (June 2014) (2013).

[46] SJL Sullivan, LDT. Topoleski, Surface modifications for improved wear performance in artificial joints: a review, JOM 67 (11) (2015) 2502–2517.

[47] NM Baloyi, API Popoola, SL. Pityana, Microstructure, hardness and corrosion properties of laser processed Ti6Al4V-based composites, Trans. Nonferrous Met. Soc. China 25 (9) (2015) 2912–2923, https://doi.org/10.1016/S1003-6326(15)63917-6 [Internet]Available from:.

[48] A Contreras, C León, O Jimenez, E Sosa, R. Pérez, Electrochemical behavior and microstructural characterization of 1026 Ni-B coated steel, Appl. Surf. Sci. 253 (2) (2006) 592–599.

[49] R Alias, R, Abd Mahmoodian, MH. Shukor, Development and characterization of a multilayer silver/silver-tantalum oxide thin film coating on stainless steel for biomedical applications, Int. J. Adhes. Adhes. 92 (April) (2019) 89–98, https://doi.org/10.1016/j.ijadhadh.2019.04.010 [Internet]Available from:.